Catalysis Science & Technology

rsc.li/catalysis

ROYAL SOCIETY
OF CHEMISTRY
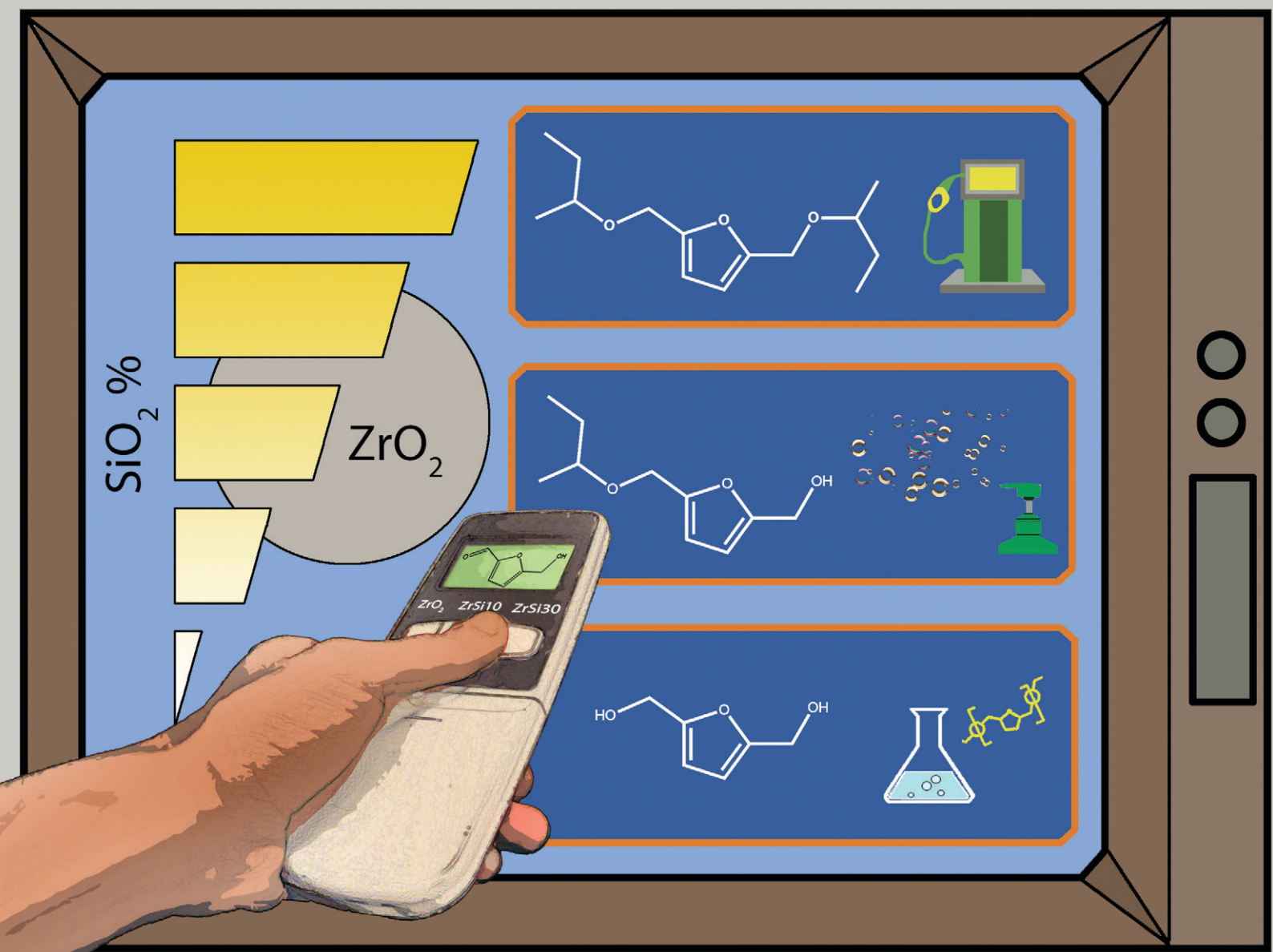
PAPER
Nicola Scotti *et al.*
On demand production of ethers or alcohols from furfural and
HMF by selecting the composition of a Zr/Si catalyst

PAPER

Check for updates

On demand production of ethers or alcohols from furfural and HMF by selecting the composition of a Zr/Si catalyst†

Federica Zaccheria,[a] Filippo Bossola, [iD][a] Nicola Scotti, [iD]*[a] Claudio Evangelisti,[b] Vladimiro Dal Santo[a] and Nicoletta Ravasio [iD][a]

Zr/Si mixed oxides with different amounts of silica (0–50 wt%) were prepared by a simple sol–gel method. These catalysts were tested in a cascade reaction of furfural and 5-hydroxymethyl furfural (HMF) with 2-butanol to form the corresponding alcohols or ethers through a combination of transfer hydrogenation and etherification processes under mild conditions. The selectivity can be finely tuned by changing the silica content which heavily impacts the acid–base properties. On pure ZrO_2, featuring acid–base pairs, only the catalytic transfer hydrogenation occurs leading to alcohol products. In contrast, on ZrSi30 the etherification reaction is strongly favored owing to near one-to-one Lewis and Brønsted acid sites. Ethers can thus be produced in high yields (≥90%), in particular the highly valuable diether of 5-hydroxymethyl furfural. The catalysts were characterized by N_2 and CO_2 absorption isotherms, FT-IR of adsorbed pyridine, 2-propanol TPD, and STEM-EDX mapping. For the first time we show that the tuning of acid–base properties by simple silica addition, with the somewhat unexpected rise of Brønsted acidity, may represent the starting point for the development of cheap but highly active and selective catalysts for furfural and HMF transformation.

Introduction

In the search for a renewable source able to significantly reduce the anthropogenic carbon footprint on a global scale, lignocellulose is the most promising feedstock due to its abundance and non-food character. Lignocellulose is a prolific material being the starting point for the synthesis of a wide range of aliphatic and aromatic compounds that are commonly derived from the traditional petrol-based chemistry.[1–5]

Among the compounds derived from the upgrading of the polysaccharide-based fractions of lignocellulose, furfural and 5-hydroxymethyl furfural (HMF) stand out as they are versatile platform molecules that could be further transformed to obtain promising biofuels, chemicals, and polymers precursors.[6,7]

Two of the main derivatives of furfural and HMF are respectively furfuryl alcohol and 2,5-bis(hydroxymethyl)furan (BHMF). Both of them find a wide application area, ranging from fine chemistry, to pharmaceuticals, polymers, solvents, lubricants and biofuels. They can be prepared through traditional hydrogenation systems by using molecular hydrogen (furfuryl alcohol is industrially produced over toxic copper-chromite catalysts) or by catalytic transfer hydrogenation (CTH) processes.[7–9]

Environmentally acceptable direct hydrogenation catalysts for the transformation of furfural and HMF into related alcohols or diols are based on nanoparticles of Cu, Pd, Pt, Ru, Au, Co, and Ni.[6,7,10–27]

Catalytic systems that don't require the use of molecular hydrogen are considered even more sustainable alternatives for the hydroupgrading of biomass-derived molecules, such as furfural and HMF, allowing substantial reduction of the complexity of production systems and therefore the costs.[9]

Also the reaction selectivity can be improved if CTH occurs through a concerted Meerwein–Ponndorf–Verley (MPV) mechanism, that is without the evolution of molecular hydrogen, by which the reduction has an exclusive selectivity towards the transformation of a carbonyl group into a hydroxyl group.[28]

Different catalytic systems active in the CTH processes of furfural and HMF for the synthesis of furfuryl alcohol and BHMF are reported in the literature. Alongside precious metal and/or expensive complicated materials,[29–40] cheaper catalysts based on Cu, Co, Fe, Hf, Mn, Zr, or zeolites (*e.g.* Sn- and Zr-beta) are also reported.[25,29,32,41–60]

[a] CNR, Istituto di Scienze e Tecnologie Chimiche "Giulio Natta" (SCITEC), via Golgi 19, 20133 Milano, Italy. E-mail: nicola.scotti@scitec.cnr.it
[b] CNR, Istituto di Chimica dei Composti Organometallici (ICCOM), via G. Moruzzi 1, 56124 Pisa, Italy
† Electronic supplementary information (ESI) available. See DOI: 10.1039/d0cy01427c

7502 | *Catal. Sci. Technol.*, 2020, **10**, 7502–7511

This journal is © The Royal Society of Chemistry 2020

Alcohols are attractive compounds for CTH reactions being at the same time a solvent and a hydrogen-donor combined with their low cost, renewable nature and unique ability to participate in intra- and intermolecular hydrogen transfers.[9] The presence of an alcohol in the reaction medium also favors the etherification reaction which leads to a different class of interesting molecules. Indeed, the ethers of furfural and HMF could be used as biofuels in diesel blends as cetane boosters.[7,8,61–65]

In the case of HMF, the direct acid-catalyzed etherification of the hydroxyl group forms a monoether, but the remaining carbonyl group negatively impacts the fuel grade of the resulting molecules. To improve the stability and the miscibility with diesel, the aldehyde group of HMF must be functionalized as an ether, making the diether the most desirable product. Whereas the production of monoethers, which has been studied quite extensively, is far easier,[66–73] the diether synthesis is troublesome, involving a reduction step prior to etherification.[51,74–76]

The same applies for furfural, where the preparation of ethers requires the combination of a reduction step followed by the etherification of the resulting alcohol.[77–79]

Some examples of the synthesis of furfuryl ethers and HMF diethers have been reported in the literature.[17,31,51,58,61,62,74–76,80–85] One strategy consists in using a mechanical mixture of a reduction catalyst with an acid one.[16,31,62,83] In order to further improve the productivity and the selectivity of the desired ethers, the hydrogenation and etherification activity can be conveniently combined using a unique bifunctional heterogeneous material.[17,74–76,80–82,84,85] This is particularly promising when associated with a H_2-free CTH process,[74–76,84,85] even if high ether yields (>90%) are rarely reported.[84]

The full control of the selectivity of the process is hence mandatory to completely exploit the potentiality of CTH vs. etherification reactions. Depending on the desired product that we want to obtain, the catalyst has to be designed to selectively produce one product or another, while keeping the activity as high as possible. Some of us already studied different commercial catalysts for the CTH of furfural to furfuryl alcohol.[51] We observed that solids bearing acid–base pairs on the surface, such as ZrO_2, promote only the CTH of the carbonyl group by the MPV mechanism forming furfuryl alcohol in high yields. In contrast, catalysts with a genuine Lewis acid character, such as a 5% zirconia–silica mixed oxide, features fairly good selectivity towards ethers but with a moderate 64% yield.

In this work we prepared different Zr/Si oxides by a simple sol–gel method, and we changed the relative silica content (0–50 wt%) with the aim of having precise control over reaction selectivity to obtain "on demand" production of furfuryl alcohol/BHMF or ether/diether starting from furfural/HMF under mild conditions (120 °C). 2-Butanol was used as the solvent, the hydrogen donor and the reactant, being the ether moiety precursor.

Experimental

Materials

All chemicals and materials used as supports were obtained from Sigma-Aldrich, except for HMF (≥95%) that was purchased from AVA Biochem.

Catalyst preparation

The zirconia–silica supports were prepared by a sol–gel procedure.[86] First, zirconyl chloride ($ZrOCl_2$), 30% solution in HCl (13 mL), was diluted to 100 mL with deionized water; such solution was then added dropwise at room temperature to 200 mL of an aqueous solution of ammonia at pH of 12 to obtain hydrous zirconia. A solution of tetraethylorthosilicate : 2-propanol : water (1 : 6 : 2 molar ratio, respectively) was added to hydrous zirconia and the suspension was vigorously stirred for 3 days at 75 °C. The so-obtained solid was thoroughly washed with deionized water until pH neutral, followed by drying overnight at 110 °C in air. Finally, the solid was calcined at 350 °C for 4 h in air. Five supports were prepared with different nominal amounts of silica (0, 3, 10, 30, and 50 wt% –hereafter named ZrO_2, ZrSi3, ZrSi10, ZrSi30 and ZrSi50). In order to avoid any silicon contamination from the glass containers, a Teflon container was used to prepare the pure zirconia support.

Catalyst characterization

The FT-IR studies of pyridine adsorption and desorption were carried out with an FTS-60 spectrophotometer equipped with a mid-IR MCT detector purchased from BioRad. The experiments were performed on a sample disk (15–20 mg) after simple dehydration treatment at 270 °C (20 min in air + 20 min under vacuum). A background spectrum prior to adsorption was obtained and subtracted from the subsequently recorded spectra. The adsorption of the probe molecules was carried out at room temperature, and desorption steps were performed at different temperatures from RT to 300 °C. All the spectra were reported after being normalized by the disk weight.

Transmission electron microscopy (TEM) analysis was performed using a ZEISS LIBRA200FE microscope equipped with a 200 kV FEG source. Energy-dispersive X-ray elemental maps and spectra (EDS – Oxford INCA Energy TEM 200) were collected along with HAADF-STEM (high angle annular dark field scanning transmission electron microscopy) images. The specimens were finely smashed in an agate mortar, suspended in isopropanol and sonicated, then each suspension was dropped onto a lacey carbon-coated copper grid (300 mesh) and the solvent was evaporated.

The specific surface area (SSA, BET method) of the samples was measured after evacuation of the sample (ca. 0.1 g) at 200 °C for 2 h, by collecting N_2 adsorption/desorption isotherms at −196 °C using a Micromeritics ASAP2020 surface area analyzer.
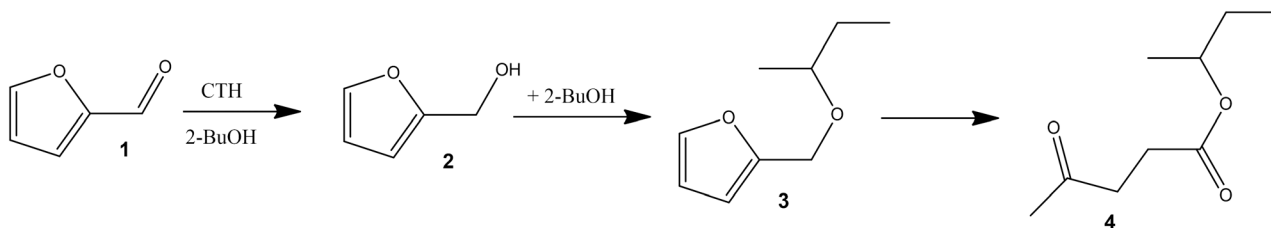
Scheme 1 Reaction pathway of furfural.

The adsorption isotherms of CO_2 were collected at RT using a Micromeritics ASAP2020 instrument, after evacuation of the sample (*ca.* 0.1 g) at 200 °C for 2 h.

2-Propanol temperature programmed desorption (IPA-TPD) experiments were carried out with a home-made apparatus described elsewhere[87] and connected downstream to a mass spectrometer (Hiden Analytical, HPR20). The samples (200 mg) were treated in a He flow (30 mL min^{-1}) at 270 °C for 40 minutes. After cooling down to 40 °C, the samples were saturated with 2-propanol, followed by 1 h under a He flow to remove the excess and physisorbed propanol. The temperature was then ramped up to 350 °C at 10 °C min^{-1} under the same carrier gas flow.

Catalytic tests

Before catalytic testing, 100 mg of catalyst were dehydrated at 270 °C (20 min in air + 20 min under vacuum) in a glass reactor, then a solution containing 100 mg of furfural or HMF and 6.2 g of 2-butanol was added at RT. The reactor was purged with vacuum, filled with 1 atm of N_2 and then placed into an oil bath at 120 °C (temperature of the bath = 125 °C) under stirring (1000 rpm).

The reaction products were analyzed by GC-FID and GC-MS (using a 5%-phenyl-methyl polysiloxane capillary column), with and without BSTFA (*N,O*-bis(trimethylsilyl) trifluoroacetamide) functionalization.
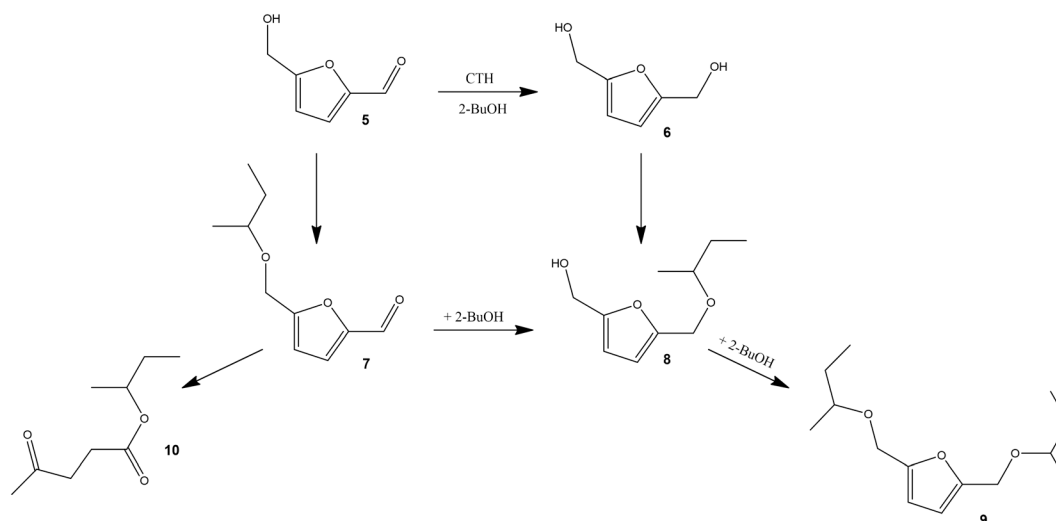
Results

General mechanism of furfural/HMF transformation

Under our experimental conditions the process of furfural/HMF transformation involves mainly the reactions of CTH and etherification, while the opening of the furan ring has been observed only to a limited extent. 2-Butanol simultaneously acts as the solvent, the hydrogen donor and the co-reactant in the etherification processes, being the precursor of the ether moiety.

On solid catalysts like ZrO_2, it is well-accepted that the CTH reaction follows a concerted MPV mechanism.[9,38,51]

In the case of furfural (Scheme 1) the carbonyl group undergoes CTH to give the corresponding alcohol **2**, as the first step, then the etherification reaction with 2-butanol eventually takes place to form 2-butyl furfuryl ether **3**. Finally, if the hydrolytic opening of the furan ring occurs, the formation of the levulinate ester **4** is also observed.[88]

On the other hand, HMF bears C=O and –OH functional groups where the reaction may start (Scheme 2). The carbonyl group is transformed into a hydroxyl group through a CTH reaction, while the –OH group undergoes etherification by reacting with 2-butanol. Thus, by a combination of H-transfer and etherification, it is possible to obtain the monoether **8** or the diether, 2,5-bis(isobutoxymethyl)furan **9**, while the sole direct etherification gives the monoether **7**. When the

Scheme 2 Reaction pathway of HMF.

7504 | *Catal. Sci. Technol.*, 2020, **10**, 7502–7511

This journal is © The Royal Society of Chemistry 2020

H-transfer is the only active process, the diol **6** (BHMF) is formed.[61]

Furfural

The reaction with furfural gives two main products, namely furfuryl alcohol and 2-butyl furfuryl ether (Scheme 1). Pure ZrO_2 (Table 1) produces the alcohol in a quantitative yield in 4 h at 120 °C, in agreement with the results that we previously reported on commercial zirconia.[51]

With the introduction of silica in the catalysts, the selectivity to the alcohol decreases in favor of the ether. In the case of ZrSi3 and ZrSi10 catalysts a mixture of alcohol and ether is formed (Table 1). The presence of silica favors also the formation of 2-butyl levulinate **4** as a side-product, especially with ZrSi3, where it reaches 7.5%. These two catalysts are not strongly selective towards the ether, but the presence of silica has a clear effect on the product distribution.

The best performing catalyst is ZrSi30. In this case the reaction goes to completion within 4 h with a remarkable selectivity towards the ether of 95%. Interestingly, with ZrSi30 the furfuryl alcohol **2** has not been observed in the reaction mixture, different from what happens with ZrSi3 and ZrSi10 (Fig. 1).[74,89]

The very different activity between ZrSi30 and ZrO_2 could be further brought to light by performing the reaction using directly furfuryl alcohol as a reactant. Indeed the former catalyzes the formation of the ether, while we already reported that zirconia is inactive.[51]

A physical mixture of ZrO_2 and SiO_2 leads to the formation of furfuryl alcohol **2** as the only product, highlighting the importance of the structure of mixed ZrSi oxides (Table S1†) in addressing the reaction towards the formation of the ether.

Using a different secondary alcohol, such as 2-octanol, ZrSi30 forms the corresponding ether (Y = 90% in 4 h), while over a primary alcohol (1-butanol) the acetal is observed as the major product, alongside a low amount of ether and an unidentified compound (Table S1†). As expected, with a tertiary alcohol (*tert*-butanol) the reaction does not proceed since it cannot undergo the CTH process (Table S1†).

5-Hydroxymethyl furfural

Starting from HMF (Table 2) we observed the formation of three main products: the diol (2,5-bis(hydroxymethyl) furan **6** –
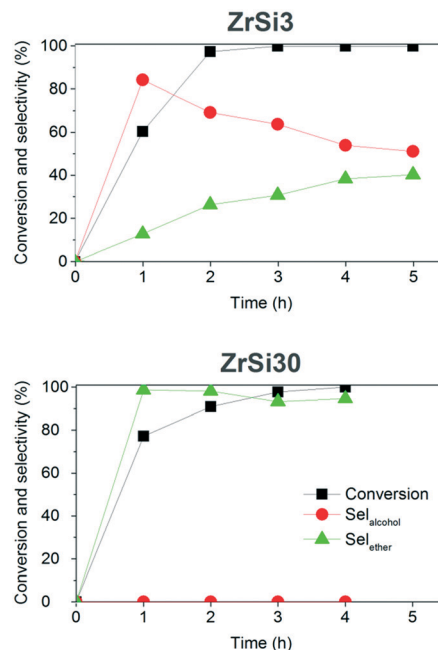

Fig. 1 Reaction profiles for furfural transformation over ZrSi3 and ZrSi30.

BHMF), the monoether of the diol (5-isobutoxymethylfurfuryl alcohol, **7**) and the diether **9**. It is significant to note that, under our experimental conditions, the product of direct etherification of HMF, 5-(isobutoxymethyl)furfural **7**, has not been observed in the reaction mixture, suggesting that HMF is less prone to etherification if compared to BHMF. A similar behavior was already described in the literature, but in that case a small amount of **7** forms in the reaction mixture.[74] Only by carrying out the reaction with a tertiary alcohol (*tert*-butanol), instead of 2-butanol, we observed the formation of 5-(*tert*-butoxymethyl) furfural as a unique product. This might be related to the absence of a H-donor molecule that prevents CTH from occurring, therefore providing indirect confirmation of the accepted mechanism for the formation of products **8** and **9**.[61]

Once again the selectivity of the process strongly depends on the silica amount. ZrO_2 has a selectivity of 100% towards BHMF **6** and in 8 h the diol yield is slightly lower than 90%. As observed with furfural, the introduction of silica promotes the etherification reactions, and the products **8** and **9** increase with the silica content. The main product with ZrSi3 is BHMF **6**, even though a small amount of monoether **8** forms. Differently, ZrSi10 shows a quite good selectivity to the monoether **8** (76.4%), and the diether **9** remains below 10%. The monoether **8** is an interesting intermediate for the synthesis of anionic surfactants derived from carbohydrates since the residual hydroxyl group can be sulfonated. However, the direct etherification of BHMF with 1-dodecanol in the presence of several Brønsted acids gave very poor results, the best yield of 10% being obtained in the presence of Amberlyst 15.[90]
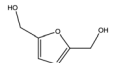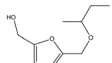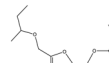
ZrSi30 is confirmed to be the most appealing catalyst, since in 7 h it forms the diether **9** in high yield, namely 96.2% (C =

Table 1 Furfural transformation over Zr-based catalysts after 4 h

Catalyst	C (%)	S_2 (%)	S_3 (%)
ZrO_2	100	100	0
ZrSi3	100	54	38
ZrSi10	100	73	26
ZrSi30	100	0	95

Table 2 HMF transformation over Zr-based catalysts

Catalyst	t (h)	C (%)	S_6 (%)	S_8 (%)	S_9 (%)
ZrO$_2$	8	89.5	100	0	0
ZrSi3	7	94.7	91.2	8.8	0
ZrSi10	7	86.3	14.5	76.4	7.4
ZrSi30	3	74.6	0.4	8.0	89.1
ZrSi30	7	97.9	0	1.5	98.5
ZrSi50	3	11.5	0	5.2	81.7

97.9%, S = 98.5%). To the best of our knowledge this is the highest yield reported for the diether of HMF obtained in the absence of molecular H$_2$, with a single catalyst.[61,74–76,84,85] Only Wei *et al.*[84] reported an 80% yield in the same ether over an SBA-15 supported ZrO$_2$ catalyst using 2-butanol. As already mentioned, the diether is a higher value-added product compared to the monoether, due to its better miscibility with diesel and its higher stability, although it is more difficult to produce.[61,74–76] It is noted that the amount of BHMF **6** detected with ZrSi30 during the entire reaction time is very low (0.7% maximum at 1 h) (Fig. S2†). A further increase in the silica content was detrimental to the activity of the resulting catalyst (Table 2, ZrSi30 *vs.* ZrSi50, 3 h).

Catalyst recycling

In light of the good performance of the ZrSi30 catalyst, we evaluated its stability through recyclability tests.

In a typical test the catalyst has been separated from the product mixture, washed with 2-butanol and dehydrated at 270 °C before the next run (20 min air + 20 min vacuum). Fig. S3† shows that ZrSi30 can be used at least four times without observing any significant loss in activity.

Influence of the catalyst features on activity and selectivity

The distinct Zr/Si composition is the reason behind the different ability of the catalysts in promoting CTH and etherification reactions. The silica content reflects on the surface area of the materials, and in particular on the structural and acid–base properties. The introduction of a simple, cheap, available and non-toxic element, such as Si, allows one to drastically change the nature of both the catalytic surface and the active site. By selecting the appropriate Zr/Si ratio the output of the reaction can be selectively shifted from the alcohol to the ether, under the same experimental conditions. As previously mentioned, a simple physical mixture of ZrO$_2$ and SiO$_2$ does not lead to the formation of the ether.

All the materials show high SSA (Table 3) that positively impacts their catalytic activity, although the preparation of high surface area zirconia is not an easy task because of its low thermal stability. The introduction of Si clearly leads to a gradual increase in SSA as already observed.[86,91]

The HAADF-STEM/EDX mapping of ZrSi3, ZrSi10 and ZrSi30 (Fig. 2) revealed no segregation of both zirconium and silicon in the catalyst grains, but rather highly homogeneous dispersion of two oxide phases, forming uniform high-surface area materials. While in the ZrO$_2$ catalyst no elements other than Zr and O were found,[91] it is very interesting to note that on ZrSi30 EDX semiquantitative analysis revealed that the Zr/Si molar ratio is almost one-to-one, in agreement with the nominal Zr/Si weight composition of this sample (Fig. S4†). A complete XPS investigation of the Zr/Si ratios has been carried out on the very same materials by some of us.[91] The results confirm the nominal Zr/Si composition and specifically the one-to-one ratio in the ZrSi30 catalyst.

The role of Lewis and Brønsted acid sites is crucial for the product distribution, and it is often debated in the literature. It is reported that Lewis acid sites promote CTH by the MPV mechanism, while it is well-known that Brønsted acidity favors the –OH etherification reaction. However, strong Brønsted acid sites may cause side-reactions, such as the hydrolytic ring-opening to form levulinate products, especially at high reaction temperature.[28,61,65,71,72,74,75,92] Hence, a material constituted only by Brønsted acid sites should be effective for direct etherification to form product **7**, being unable to activate the hydrogen transfer process. In contrast, hydrogen transfer by the MPV mechanism is favored over solid catalysts with a Lewis acid site and a neighboring base site.[9] In a previous study, some of us reported that pure Lewis acid solids, such as Cu/SiO$_2$ prepared by a chemisorption–hydrolysis method, express limited activity in the CTH of furfural and low selectivity, due to ether formation, but catalysts with acid–base pairs, such as ZrO$_2$, are definitely more active and selective.[51] In some cases, pure Lewis acidity accounts also for ether formation,[28,72,74] even though the mechanism is still poorly understood.[75,93]

Table 3 Surface area of the Zr-based materials

Catalyst	SSA (m^2 g^{-1})
ZrO$_2$	222
ZrSi3	281
ZrSi10	309
ZrSi30	353

7506 | *Catal. Sci. Technol.*, 2020, **10**, 7502–7511

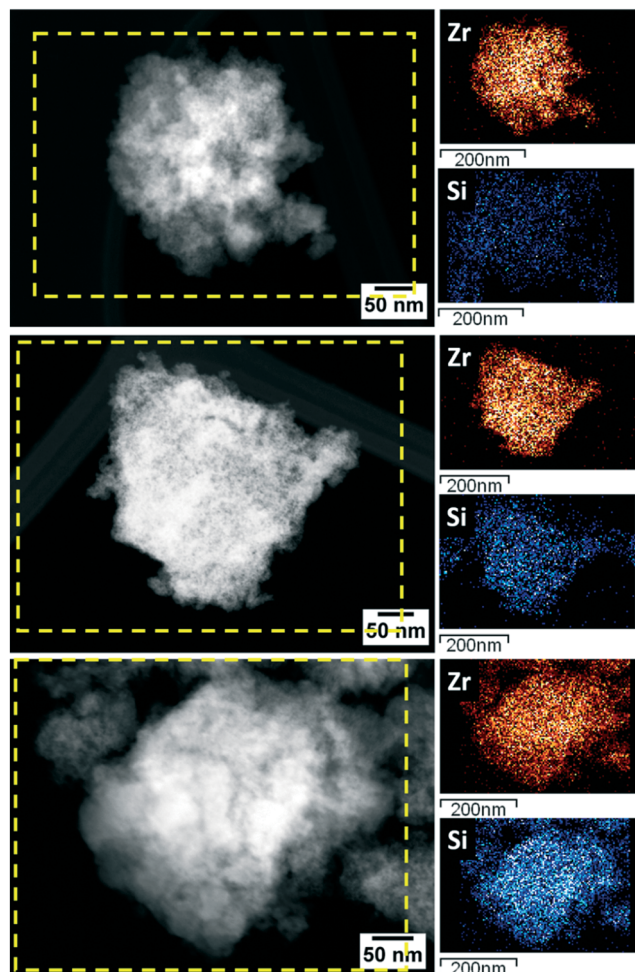This journal is © The Royal Society of Chemistry 2020

Fig. 2 HAADF-STEM image of the representative catalyst grain of ZeSi3 (top), ZeSi10 (medium) and ZrSi30 (bottom) with EDX mapping area (yellow dashed lines) and the corresponding Zr map (red) and Si map (blue).

The properties of binary oxides differ significantly, often in an unexpected way, from those of the bulk single components. The acid–base properties depend on the nature and the ratio between the two mother oxides.[94–97]

By FT-IR of adsorbed pyridine it is possible to distinguish between Lewis and Brønsted acid sites, while a weak interaction between the catalyst and the probe molecule (physisorption or hydrogen bonding) can be excluded above 100 °C.[98–102] The results, collected at the reaction temperature, namely 120 °C, are reported in Fig. 3, whilst the quantitative analysis,[103] to determine the amount of adsorbed pyridine ($mmol_{Py} \, g_{cat}^{-1}$), is reported in the inset of Fig. 3. Data show a very interesting trend: while ZrO_2 shows only Lewis sites (bands at 1448 and 1610 cm^{-1}), the introduction of silica generates Brønsted acidity (bands at 1550 and 1640 cm^{-1}) on ZrSi10, but especially on ZrSi30. It is worth noting that the ZrSi30 catalyst possesses a near one-to-one ratio between Lewis and Brønsted acid sites, which well matches with the surface molar Zr/Si composition of the material, calculated by EDX mapping. On ZrSi50 the population of both Lewis and Brønsted acid sites drops.
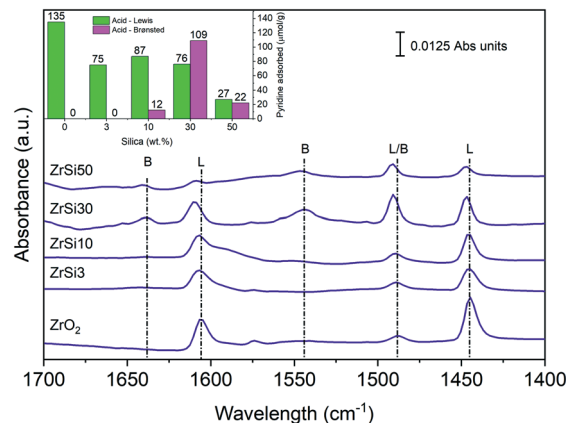

Fig. 3 FT-IR pyridine desorption spectra at 120 °C normalized by the disk weight; inset: quantitative analysis at 120 °C.

The analysis of the –OH region in the FT-IR spectra (Fig. 4) of the catalysts offers further insights into their structure. On pure ZrO_2, the less-pronounced bands at 3669 and 3777 cm^{-1} are due to hydroxyl groups over a monoclinic zirconia phase, while the one at 3728 cm^{-1} is ascribed to –OH groups over tetragonal zirconia,[104,105] in agreement with the XRD analysis already reported by some of us.[91] Different is the case of ZrSi30, where we can find only an intense band at 3740 cm^{-1} corresponding to isolated –OH groups over Si, like those typical of pure silica.[106] This means that the –OH groups on the surface of ZrSi30 resemble those of silica. A similar pattern is observed on ZrSi50 (not reported).

Silica is generally known to be a non-acidic material and needs to be modified to exhibit acidic behavior. Indeed, in our case, already with the addition of few silica, that is ZrSi3, the total population of Lewis sites drops from 135 to 75 $\mu mol_{Py} \, g^{-1}$. This would make ZrSi30 and ZrSi50 less acidic materials. This is true for ZrSi50, while it turns out that ZrSi30 has remarkable acidic properties in the form of both Lewis and Brønsted sites.

It is generally accepted that Brønsted acidity favors alcohol dehydration reactions,[107,108] but a DFT study on a SiO_2–Al_2O_3

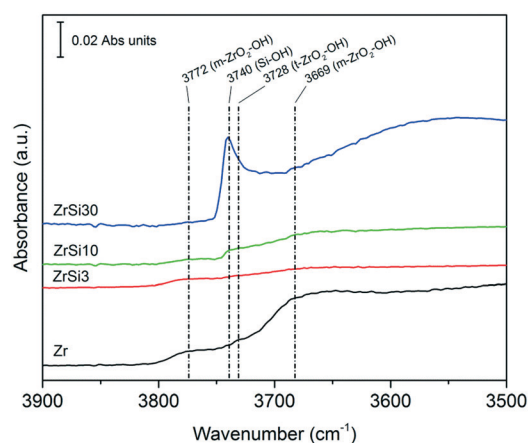**Fig. 4** FT-IR of the ZrSi catalysts, –OH region, normalized by the disk weight.

This journal is © The Royal Society of Chemistry 2020

Catal. Sci. Technol., 2020, **10**, 7502–7511 | **7507**

catalyst in 2-propanol dehydration (a common reaction used to probe the surface acidity of solid materials) suggests that the process is extremely favored on terminal silanols that interact with neighboring, coordinatively unsaturated aluminum atoms, which may exhibit Lewis acidic properties.[109] This is particularly interesting because these pseudo-bridging silanol groups enable the formation of propene through synergy between Lewis and Brønsted catalysis.

Therefore, the 2-propanol TPD represents an informative analysis to better describe our catalyst (Fig. 5). On ZrSi30 propene is formed just from 180 °C, with the maximum at 220 °C. On the other hand, the profile of ZrO_2 shows that the propene production is shifted by more than 100 °C above, with the maximum at 340 °C, indicating very different acidity. The easier formation of propene on ZrSi30 confirms the presence of Brønsted acid sites (in agreement with pyridine), but the cooperative role of Brønsted and Lewis acidity in olefin formation is also suggested from the work of Larmier *et al.*[109]

As described before, it is possible to effectively recycle the catalyst after regeneration treatment at 270 °C (20 min air + 20 min vacuum). The FT-IR analysis of pyridine on the recovered and dehydrated ZrSi30 catalyst (Fig. S5†) shows that both Lewis and Brønsted acid sites are regenerated, granting the possibility to reuse the material.

In order to have a full picture of the acid–base features of the catalysts, we measured the adsorption isotherms of CO_2, from which we calculated the number of basic sites (μmol g^{-1}). In Fig. 6 we plotted the composition in terms of basic and acid sites of the investigated catalysts. It is evident that the dramatic effect of silica extends also to the basic character of the materials. In particular, as the silica content increases, the number of basic sites quickly drops. It is interesting to note that ZrSi30 is free of basic sites and as such it can be considered as a pure solid acid. The poor catalytic activity of ZrSi50 is the result of the decrease of both acidity and basicity.

From these characterizations, it turns out that the addition of silica impacts both acid (quantity and type) and basic
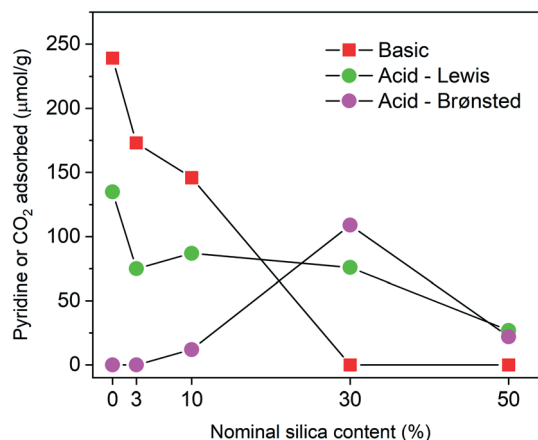

Fig. 6 Acid and basic sites (μmol g^{-1}) of all the materials.

sites (Fig. 6). The combined effect of acid–base sites drives the selectivity of the reaction from a simple CTH process to a combined CTH + etherification one. This behavior is particularly clear on HMF: ZrO_2 and ZrSi3 form BHMF **6** in high yields as the Lewis acid–base pairs are predominant; differently, in ZrSi10 and ZrSi30, the concurrent and gradual effect of the decrease of basic sites and the increase of Brønsted acid sites, pushes towards the formation of ethers. The catalyst with a moderate amount of both basic sites and Brønsted acid sites, namely ZrSi10, is selective for the monoether **8**, whereas ZrSi30, which combines Lewis and Brønsted acid sites without the basic ones, produces the diether **9** in a 96.4% yield.

With furfural ZrSi3 and ZrSi10 behave in a similar way, whereas ZrO_2 and ZrSi30 confirm their complementary role in the upgrade of this compound, giving selectively furfuryl alcohol **2** and 2-butyl furfuryl ether **3**, respectively.

From the correlation between the characterization and the catalytic data, we can speculate on the reaction mechanism. On ZrSi10 and ZrSi30 HMF is first adsorbed on a Lewis acid site where the reaction proceeds through the MPV mechanism to form BHMF **6**. Then the etherification reaction takes place, promoted in particular by a Brønsted acid site, to form the product **8** and eventually the diether **9**. This mechanism explains the reaction profiles and especially the absence of monoether **7** in the product mixture for each reaction time.

We propose that ZrSi30 is a material where the Lewis acid site, as Zr^{4+}, accounts for the first adsorption of the reactant (furfural or HMF) which is consequently transformed into the corresponding alcohol/diol by a CTH reaction. The so-formed alcohol is now prone to etherification that it is strongly favored by the Brønsted acidity. The CTH process over ZrO_2 is enhanced by the presence of acid–base pairs, while that over ZrSi30 is favored by the quick transformation of BHMF into the monoether, hence shifting the equilibrium of the reaction and also preventing the formation of side-products.

Our hypothesis is that the high surface area and the homogeneity of the materials in terms of Zr and Si inter-
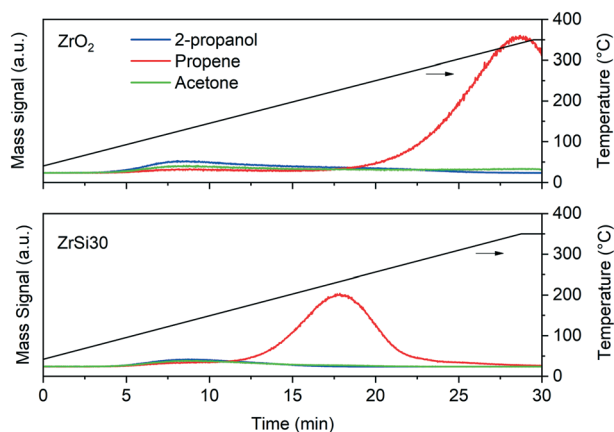

Fig. 5 2-Propanol TPD of ZrO_2 and ZrSi30.

dispersion lead to the formation of a Zr–O–Si network that is the basis of the peculiar features of ZrSi30, with a near one-to-one ratio between Lewis and Brønsted acidity. Pyen et al.[108] had investigated similar materials finding comparable acidic properties and concluded on the basis of XPS characterization that Brønsted sites are constituted of Zr–OH groups. FT-IR investigations, however, did not reveal any bands ascribable to such groups in our catalyst featuring Brønsted acidity (Fig. 4). Furthermore, in previous studies on zirconia–silica mixed oxides[108,110] the electron density on oxygen, which is related to the acidic properties, has been reported to increase upon addition of silica. But, in another work by some of us,[91] we found a lower electron density on the oxygen in similar materials, resembling very much what was described by Hong et al.[111] They argued that such oxygens are part of surface –OH groups with slight Brønsted character and bond to oxygen vacancies as revealed by the Zr XPS peaks. As described in our aforementioned work[91] , though, we did not find any evidence of such vacancies and, in fact, the Zr sites were progressively depleted of electron density with increasing silica content. All this to say that the search for the actual Brønsted site is still ongoing and not so trivial.

The fact that upon silica addition the Lewis acid sites decrease in number but then remain constant up to the nominal 30% of SiO_2, along with the appearance of Brønsted sites only with a specific silica quantity, highlights the role of the structure at the atomistic scale of the material on their final acidic properties. It is clear that the positive identification of the Brønsted site is of primary importance to master the acidic properties of these highly interesting silica–zirconia materials, and indeed is currently under deep investigation.

Conclusions

For the first time, we show that with the addition of silica to a ZrO_2 oxide it is possible to tune the acid–base properties of the resulting catalyst and so the selectivity in the transformation of furfural and HMF into the corresponding alcohols or ethers. Moving from ZrO_2 to ZrSi30, it is possible to change the output of the reaction from furfuryl alcohol **2** and BHMF **6** to 2-butyl furfuryl ether **3** and 2,5-bis(isobutoxymethyl)furan **9**. The yields of the products are excellent (≥90%) and the reaction conditions are mild. In particular, ZrSi30 is an effective multifunctional material for the exclusive synthesis of ethers from furfural and HMF, with a yield respectively of 94.6% and 96.2%. To the best of our knowledge, such high yield values represent a step toward the production of these furan-based cetane boosters, considering that the process occurs without the need of molecular hydrogen and with a catalyst that is simple to prepare, cheap and noble metal-free.

The key to the activity of ZrSi30 is the near one-to-one Lewis–Brønsted sites that are involved respectively in the CTH and etherification reactions. The presence of Brønsted acidity

is simply achieved by the addition of silica but, however critical, remains elusive and is worthy of deeper investigation.

It is also worth noting that, from HMF, ZrSi10 gives the monoether **8** as the main product. This is an interesting intermediate for the synthesis of anionic surfactants due to its residual hydroxyl group, while in the literature it is usually reported the preparation of monoether **7**,[66–73] which can be used as biofuel, but having worse properties compared to the diether.

Conflicts of interest

There are no conflicts to declare.

Acknowledgements

References

1 R. A. Sheldon, *Green Chem.*, 2014, **16**, 950–963.

2 D. Esposito and M. Antonietti, *Chem. Soc. Rev.*, 2015, **44**, 5821–5835.

3 C. Xu, R. A. D. Arancon, J. Labidi and R. Luque, *Chem. Soc. Rev.*, 2014, **43**, 7485–7500.

4 S. De, S. Dutta and B. Saha, *Catal. Sci. Technol.*, 2016, **6**, 7364–7385.

5 D. M. Alonso, S. G. Wettstein and J. A. Dumesic, *Chem. Soc. Rev.*, 2012, **41**, 8075–8098.

6 X. Li, P. Jia and T. Wang, *ACS Catal.*, 2016, **6**, 7621–7640.

7 F. A. Kucherov, L. V. Romashov, K. I. Galkin and V. P. Ananikov, *ACS Sustainable Chem. Eng.*, 2018, **6**, 8064–8092.

8 R. Mariscal, P. Maireles-Torres, M. Ojeda, I. Sádaba and M. López Granados, *Energy Environ. Sci.*, 2016, **9**, 1144–1189.

9 M. J. Gilkey and B. Xu, *ACS Catal.*, 2016, **6**, 1420–1436.

10 M. M. Villaverde, N. M. Bertero, T. F. Garetto and A. J. Marchi, *Catal. Today*, 2013, **213**, 87–92.

11 M. Ghashghaee, S. Sadjadi, S. Shirvani and V. Farzaneh, *Catal. Lett.*, 2017, **147**, 318–327.

12 D. Vargas-Hernández, J. M. Rubio-Caballero, J. Santamaría-González, R. Moreno-Tost, J. M. Mérida-Robles, M. A. Pérez-Cruz, A. Jiménez-López, R. Hernández-Huesca and P. Maireles-Torres, *J. Mol. Catal. A: Chem.*, 2014, **383–384**, 106–113.

13 A. Jouve, S. Cattaneo, D. Delgado, N. Scotti, C. Evangelisti, J. M. López Nieto and L. Prati, *Appl. Sci.*, 2019, **9**, 2287.

14 J. Ohyama, A. Esaki, Y. Yamamoto, S. Arai and A. Satsuma, *RSC Adv.*, 2013, **3**, 1033–1036.

15 M. Chatterjee, T. Ishizaka and H. Kawanami, *Green Chem.*, 2014, **16**, 4734–4739.

16 M. Balakrishnan, E. R. Sacia and A. T. Bell, *Green Chem.*, 2012, **14**, 1626–1634.

17 X. L. Li, K. Zhang, S. Y. Chen, C. Li, F. Li, H. J. Xu and Y. Fu, *Green Chem.*, 2018, **20**, 1095–1105.

18 M. Audemar, C. Ciotonea, K. De Oliveira Vigier, S. Royer, A. Ungureanu, B. Dragoi, E. Dumitriu and F. Jérôme, *ChemSusChem*, 2015, **8**, 1885–1891.

19 Y. Feng, G. Yan, T. Wang, W. Jia, X. Zeng, J. Sperry, Y. Sun, X. Tang, T. Lei and L. Lin, *Green Chem.*, 2019, **21**, 4319–4323.

20 S. M. Rogers, C. R. A. Catlow, C. E. Chan-Thaw, A. Chutia, N. Jian, R. E. Palmer, M. Perdjon, A. Thetford, N. Dimitratos, A. Villa and P. P. Wells, *ACS Catal.*, 2017, **7**, 2266–2274.

21 W. Gong, C. Chen, Y. Zhang, H. Zhou, H. Wang, H. Zhang, Y. Zhang, G. Wang and H. Zhao, *ACS Sustainable Chem. Eng.*, 2017, **5**, 2172–2180.

22 W. Ouyang, A. Yepez, A. A. Romero and R. Luque, *Catal. Today*, 2018, **308**, 32–37.

23 A. J. Garcia-Olmo, A. Yepez, A. M. Balu, P. Prinsen, A. Garcia, A. Maziere, C. Len and R. Luque, *Tetrahedron*, 2017, **73**, 5599–5604.

24 X. Yang, H. Chen, Q. Meng, H. Zheng, Y. Zhu and Y. W. Li, *Catal. Sci. Technol.*, 2017, **7**, 5625–5634.

25 X. Yang, X. Xiang, H. Chen, H. Zheng, Y. W. Li and Y. Zhu, *ChemCatChem*, 2017, **9**, 3023–3030.

26 C. P. Jiménez-Gómez, J. A. Cecilia, D. Durán-Martín, R. Moreno-Tost, J. Santamaría-González, J. Mérida-Robles, R. Mariscal and P. Maireles-Torres, *J. Catal.*, 2016, **336**, 107–115.

27 Q. Yuan, D. Zhang, L. Van Haandel, F. Ye, T. Xue, E. J. M. Hensen and Y. Guan, *J. Mol. Catal. A: Chem.*, 2015, **406**, 58–64.

28 J. Wei, X. Cao, T. Wang, H. Liu, X. Tang, X. Zeng, Y. Sun, T. Lei, S. Liu and L. Lin, *Catal. Sci. Technol.*, 2018, **8**, 4474–4484.

29 J. Wei, T. Wang, P. Tang, X. Tang, Y. Sun, X. Zeng and L. Lin, *Curr. Org. Chem.*, 2019, **23**, 2155–2167.

30 C. K. P. Neeli, Y. M. Chung and W. S. Ahn, *ChemCatChem*, 2017, **9**, 4570–4579.

31 P. Panagiotopoulou, N. Martin and D. G. Vlachos, *ChemSusChem*, 2015, **8**, 2046–2054.

32 J. Li, J. L. Liu, H. J. Zhou and Y. Fu, *ChemSusChem*, 2016, **9**, 1339–1347.

33 D. Scholz, C. Aellig and I. Hermans, *ChemSusChem*, 2014, **7**, 268–275.

34 J. Zhang and J. Chen, *ACS Sustainable Chem. Eng.*, 2017, **5**, 5982–5993.

35 H. Li, X. Liu, T. Yang, W. Zhao, S. Saravanamurugan and S. Yang, *ChemSusChem*, 2017, **10**, 1761–1770.

36 S. Rojas-Buzo, P. García-García and A. Corma, *ChemSusChem*, 2018, **11**, 432–438.

37 H. Li, Z. Fang, J. He and S. Yang, *ChemSusChem*, 2017, **10**, 681–686.

38 H. Li, J. He, A. Riisager, S. Saravanamurugan, B. Song and S. Yang, *ACS Catal.*, 2016, **6**, 7722–7727.

39 T. Wang, J. Zhang, W. Xie, Y. Tang, D. Guo and Y. Ni, *Catalysts*, 2017, **7**, 4–11.

40 H. Li, T. Yang and Z. Fang, *Appl. Catal., B*, 2018, **227**, 79–89.

41 W. Gong, C. Chen, Y. Zhang, H. Zhou, H. Wang, H. Zhang, Y. Zhang, G. Wang and H. Zhao, *ACS Sustainable Chem. Eng.*, 2017, **5**, 2172–2180.

42 M. M. Villaverde, T. F. Garetto and A. J. Marchi, *Catal. Commun.*, 2015, **58**, 6–10.

43 H. P. Reddy Kannapu, C. A. Mullen, Y. Elkasabi and A. A. Boateng, *Fuel Process. Technol.*, 2015, **137**, 220–228.

44 Q. Hu, G. Fan, L. Yang, X. Cao, P. Zhang, B. Wang and F. Li, *Green Chem.*, 2016, **18**, 2317–2322.

45 Y. Zhang, M. S. Gyngazova, A. Lolli, L. Grazia, T. Tabanelli, F. Cavani and S. Albonetti, in *Horizons in Sustainable Industrial Chemistry and Catalysis*, Elsevier B.V., 2019, vol. 178, pp. 195–214.

46 L. Hu, S. Liu, J. Song, Y. Jiang, A. He and J. Xu, *Waste Biomass Valoriz.*, 2020, **11**, 3485–3499.

47 T. A. Natsir, T. Hara, N. Ichikuni and S. Shimazu, *Chem. Lett.*, 2017, **46**, 1580–1583.

48 R. López-Asensio, J. A. Cecilia, C. P. Jiménez-Gómez, C. García-Sancho, R. Moreno-Tost and P. Maireles-Torres, *Appl. Catal., A*, 2018, **556**, 1–9.

49 K. S. Koppadi, R. R. Chada, S. S. Enumula, R. K. Marella, S. R. R. Kamaraju and D. R. Burri, *Catal. Lett.*, 2017, **147**, 1278–1284.

50 M. Koehle and R. F. Lobo, *Catal. Sci. Technol.*, 2016, **6**, 3018–3026.

51 N. Scotti, F. Zaccheria, C. Bisio, C. Vittoni and N. Ravasio, *ChemistrySelect*, 2018, **3**, 8344–8348.

52 J. He, L. Schill, S. Yang and A. Riisager, *ACS Sustainable Chem. Eng.*, 2018, **6**, 17220–17229.

53 J. He, H. Li, A. Riisager and S. Yang, *ChemCatChem*, 2018, **10**, 430–438.

54 M. S. Gyngazova, L. Grazia, A. Lolli, G. Innocenti, T. Tabanelli, M. Mella, S. Albonetti and F. Cavani, *J. Catal.*, 2019, **372**, 61–73.

55 M. Soo, F. Stefanus, H. Simanjuntak, S. Lim, J. Jae, J. Ha and H. Lee, *J. Ind. Eng. Chem.*, 2017, **52**, 59–65.

56 R. Ramos, A. F. Peixoto, B. I. Arias-Serrano, O. S. G. P. Soares, M. F. R. Pereira, D. Kubička and C. Freire, *ChemCatChem*, 2020, **12**, 1–10.

57 W. Hao, W. Li, X. Tang, X. Zeng, Y. Sun, S. Liu and L. Lin, *Green Chem.*, 2016, **18**, 1080–1088.

58 H. Li, Z. Fang, R. L. Smith and S. Yang, *Prog. Energy Combust. Sci.*, 2016, **55**, 98–194.

59 Y. Feng, S. Long, G. Yan, B. Chen, J. Sperry, W. Xu, Y. Sun, X. Tang, X. Zeng and L. Lin, *J. Catal.*, 2020, **389**, 157–165.

60 G. H. Wang, X. Deng, D. Gu, K. Chen, H. Tüysüz, B. Spliethoff, H. J. Bongard, C. Weidenthaler, W. Schmidt and F. Schüth, *Angew. Chem., Int. Ed.*, 2016, **55**, 11101–11105.

61 H. Nguyen, N. Xiao, S. Daniels, N. Marcella, J. Timoshenko, A. Frenkel and D. G. Vlachos, *ACS Catal.*, 2017, **7**, 7363–7370.

62 Q. Cao, W. Liang, J. Guan, L. Wang, Q. Qu, X. Zhang, X. Wang and X. Mu, *Appl. Catal., A*, 2014, **481**, 49–53.

63 D. R. Chaffey, T. E. Davies, S. H. Taylor and A. E. Graham, *ACS Sustainable Chem. Eng.*, 2018, **6**, 4996–5002.

7510 | *Catal. Sci. Technol.*, 2020, **10**, 7502–7511

This journal is © The Royal Society of Chemistry 2020

64 G.-J. Gruter and E. De Jong, *Biofuels Technol.*, 2009, pp. 11–17.

65 J. E. Rorrer, A. T. Bell and F. D. Toste, *ChemSusChem*, 2019, 2835–2858.

66 D. Hu, H. Hu, H. Jin, P. Zhang, Y. Hu, S. Ying, X. Li, Y. Yang, J. Zhang and L. Wang, *Appl. Catal., A*, 2020, **590**, 117338.

67 X. Liu and R. Wang, *Biomass, Biofuels, Biochem.*, 2020, pp. 355–375.

68 P. Lanzafame, G. Papanikolaou, S. Perathoner, G. Centi, G. Giordano and M. Migliori, *Microporous Mesoporous Mater.*, 2020, **300**, 110157.

69 E. R. Sacia, M. Balakrishnan and A. T. Bell, *J. Catal.*, 2014, **313**, 70–79.

70 M. C. Allen, A. J. Hoffman, T. Liu, M. S. Webber, D. Hibbitts and T. J. Schwartz, *ACS Catal.*, 2020, 6771–6785.

71 P. Lanzafame, K. Barbera, S. Perathoner, G. Centi, A. Aloise, M. Migliori, A. MacArio, J. B. Nagy and G. Giordano, *J. Catal.*, 2015, **330**, 558–568.

72 K. Barbera, P. Lanzafame, A. Pistone, S. Millesi, G. Malandrino, A. Gulino, S. Perathoner and G. Centi, *J. Catal.*, 2015, **323**, 19–32.

73 P. Lanzafame, G. Papanikolaou, S. Perathoner, G. Centi, M. Migliori, E. Catizzone, A. Aloise and G. Giordano, *Catal. Sci. Technol.*, 2018, **8**, 1304–1313.

74 J. Jae, E. Mahmoud, R. F. Lobo and D. G. Vlachos, *ChemCatChem*, 2014, **6**, 508–513.

75 J. D. Lewis, S. Van De Vyver, A. J. Crisci, W. R. Gunther, V. K. Michaelis, R. G. Griffin and Y. Román-Leshkov, *ChemSusChem*, 2014, **7**, 2255–2265.

76 J. Luo, J. Yu, R. J. Gorte, E. Mahmoud, D. G. Vlachos and M. A. Smith, *Catal. Sci. Technol.*, 2014, **4**, 3074–3081.

77 N. L. Mulik, P. S. Niphadkar and V. V. Bokade, *Res. Chem. Intermed.*, 2020, **46**, 2309–2325.

78 C. R. Patil and C. V. Rode, *ChemistrySelect*, 2018, **3**, 12504–12511.

79 T. A. Natsir and S. Shimazu, *Fuel Process. Technol.*, 2020, **200**, 106308.

80 R. Pizzi, R.-J. van Putten, H. Brust, S. Perathoner, G. Centi and J. van der Waal, *Catalysts*, 2015, **5**, 2244–2257.

81 Y. Wang, Q. Cui, Y. Guan and P. Wu, *Green Chem.*, 2018, **20**, 2110–2117.

82 J. Wei, T. Wang, X. Cao, H. Liu, X. Tang, Y. Sun, X. Zeng, T. Lei, S. Liu and L. Lin, *Appl. Catal., B*, 2019, **258**, 117793.

83 S. Shinde and C. Rode, *ChemSusChem*, 2017, **10**, 4090–4101.

84 J. Wei, T. Wang, H. Liu, M. Li, X. Tang, Y. Sun, X. Zeng, L. Hu, T. Lei and L. Lin, *Energy Technol.*, 2019, **7**, 1801071–1801081.

85 J. Iglesias, J. Melero, G. Morales, J. Moreno, Y. Segura, M. Paniagua, A. Cambra and B. Hernández, *Catalysts*, 2015, **5**, 1911–1927.

86 Q. Zhao, W. H. Shih, H. L. Chang and P. Andersen, *Appl. Catal., A*, 2004, **262**, 215–221.

87 V. Dal Santo, C. Dossi, A. Fusi, R. Psaro, C. Mondelli and S. Recchia, *Talanta*, 2005, **66**, 674–682.

88 L. Bui, H. Luo, W. R. Gunther and Y. Román-Leshkov, *Angew. Chem., Int. Ed.*, 2013, **52**, 8022–8025.

89 M. M. Antunes, S. Lima, P. Neves, A. L. Magalhães, E. Fazio, A. Fernandes, F. Neri, C. M. Silva, S. M. Rocha, M. F. Ribeiro, M. Pillinger, A. Urakawa and A. A. Valente, *J. Catal.*, 2015, **329**, 522–537.

90 L. Kipshagen, L. T. Vömel, M. A. Liauw, A. Klemmer, A. Schulz, C. Kropf, P. J. C. Hausoul and R. Palkovits, *Green Chem.*, 2019, **21**, 3882–3890.

91 F. Bossola, N. Scotti, F. Somodi, M. Coduri, C. Evangelisti and V. Dal Santo, *Appl. Catal., B*, 2019, **258**, 118016.

92 L. Bui, H. Luo, W. Gunther and Y. Román-Leshkov, *Angew. Chem., Int. Ed.*, 2013, **52**, 8022–8025.

93 N. Scotti, D. Monticelli and F. Zaccheria, *Inorg. Chim. Acta*, 2012, **380**, 194–200.

94 P. Kennedy, *J. Catal.*, 1992, **517**, 505–517.

95 K. Tanabe, S. Takashi and S. Katseu, *Bull. Chem. Soc. Jpn.*, 1974, **47**, 1064–1066.

96 P. K. Doolin, S. Alerasool, D. J. Zalewski and J. F. Hoffman, *Catal. Lett.*, 1994, **25**, 209–223.

97 N. Scotti, F. Bossola, F. Zaccheria and N. Ravasio, *Catalysts*, 2020, **10**, 168.

98 N. Scotti, F. Zaccheria, C. Evangelisti, R. Psaro and N. Ravasio, *Catal. Sci. Technol.*, 2017, **7**, 1386–1393.

99 N. Scotti, M. Dangate, A. Gervasini, C. Evangelisti, N. Ravasio and F. Zaccheria, *ACS Catal.*, 2014, **4**, 2818–2826.

100 G. Cre, V. Montouillout, A. Vimont, L. Mariey, T. Cseri and F. Mauge, *J. Phys. Chem. B*, 2006, **110**, 15172–15185.

101 J. N. Kondo, R. Nishitani, E. Yoda, T. Yokoi, T. Tatsumi and K. Domen, *Phys. Chem. Chem. Phys.*, 2010, **12**, 11576–11586.

102 A. Gervasini, P. Carniti, F. Bossola, C. Imparato, P. Pernice, N. J. Clayden and A. Aronne, *Mol. Catal.*, 2018, **458**, 280–286.

103 C. A. Emeis, *J. Catal.*, 1993, **141**, 347–354.

104 Z. Y. Ma, C. Yang, W. Wei, W. H. Li and Y. H. Sun, *J. Mol. Catal. A: Chem.*, 2005, **227**, 119–124.

105 R. A. L. Baylon, J. Sun, L. Kovarik, M. Engelhard, H. Li, A. D. Winkelman and Y. Wang, *Appl. Catal., B*, 2018, **234**, 337–346.

106 I. A. Isher and A. T. Bell, *J. Catal.*, 1999, **376**, 357–376.

107 C. P. Nash, A. Ramanathan, D. A. Ruddy, M. Behl, E. Gjersing, M. Griffin, H. Zhu, B. Subramaniam, J. A. Schaidle and J. E. Hensley, *Appl. Catal., A*, 2016, **510**, 110–124.

108 S. Pyen, E. Hong, M. Shin, Y. W. Suh and C. H. Shin, *Mol. Catal.*, 2018, **448**, 71–77.

109 K. Larmier, C. Chizallet, S. Maury, N. Cadran, J. Abboud, A. F. Lamic-Humblot, E. Marceau and H. Lauron-Pernot, *Angew. Chem., Int. Ed.*, 2017, **56**, 230–234.

110 H. J. M. Bosman, A. P. Pijpers and A. W. M. A. Jaspers, *J. Catal.*, 1996, **161**, 551–559.

111 E. Hong, S. W. Baek, M. Shin, Y. W. Suh and C. H. Shin, *J. Ind. Eng. Chem.*, 2017, **54**, 137–145.

This journal is © The Royal Society of Chemistry 2020

Catal. Sci. Technol., 2020, **10**, 7502–7511 | **7511**